THE JOURNAL OF PHYSICAL CHEMISTRY C

Article

pubs.acs.org/JPCC

Concavity Effects on the Optical Properties of Aromatic Hydrocarbons

Caterina Cocchi,*[,†,⊥] Deborah Prezzi,[†] Alice Ruini,[†,‡] Marilia J. Caldas,[§] Annalisa Fasolino,[∥] and Elisa Molinari[†,‡]

[†]Centro S3, CNR-Istituto Nanoscienze, I-41125 Modena, Italy

[‡]Dipartimento di Scienze Fisiche, Informatiche e Matematiche, Università di Modena e Reggio Emilia, I-41125 Modena, Italy

[§]Instituto de Física, Universidade de São Paulo, 05508-900 São Paulo, SP, Brazil

[∥]Institute for Molecules and Materials, Radboud University Nijmegen, Heyendaalseweg 135, 6525AJ Nijmegen, The Netherlands

Supporting Information

ABSTRACT: We study the modifications on the ground and excited state properties of polycyclic aromatic hydrocarbons (PAHs), induced by the variation of concavity and π-connectivity. Inspired by experimentally feasible systems, we study three series of PAHs, from H-saturated graphene flakes to geodesic buckybowls, related to the formation of fullerene C_{60} and C_{50}-carbon nanotube caps. Working within the framework of quantum chemistry semiempirical methods AM1 and ZINDO/S, we find that the interplay between concavity and π-connectivity shifts the bright optical lines to higher energies and introduces symmetry-forbidden dark excitations at low energy. A generally good agreement with the available experimental data supports our results, which can be viewed as the basis for designing optical properties of novel curved aromatic molecules.

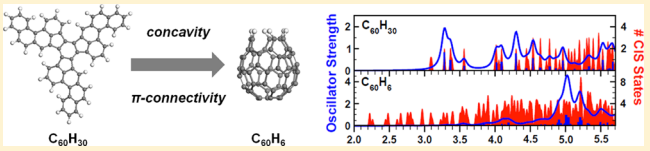

The discovery of fullerene[1] and carbon nanotubes (CNTs)[2] and, more recently, of graphene,[3] each with unique physical and chemical properties,[4,5] has promoted a continuous research on carbon nanoscience.[6] In this context, nonplanar polycyclic aromatic hydrocarbons (PAHs), including buckybowls and geodesic polyarenes, have gained increasing importance both as synthesis intermediates[7−11] and as intriguing systems themselves.[12−17] Indeed, the interest in identifying the path bringing flat aromatic molecules into fullerene cages extends also to other fields than organic chemistry, as for instance to astrochemistry.[18] In another direction, crystal-packed structures[19,20] and supramolecular compounds made of curved PAHs[21] can be nowadays synthesized with promising perspectives toward molecular nanodevices.[22−27]

Since the main features of carbon-based materials are known to be critically influenced by morphological details, including edge modifications[28−36] and structural distortions,[37−40] we here address the effects, induced by variations of concavity and π-connectivity, on the ground and excited state properties of PAHs. Inspired by the synthesis intermediates of C_{60}-fullerene and C_{50}-CNT-caps,[9,10,14,41] we study three series of symmetric PAHs, ranging from planar molecules to concave buckybowls, and compare our results with the available theoretical and experimental data.[10,14,42,43] The ground state properties of these PAHs are characterized by the appearance of a net dipole in the out-of-plane direction, as soon as the molecule starts to deviate from planarity. The optical absorption is also very sensitive to the increase of both concavity and π-connectivity, which produces a blue-shift of the bright optical lines and at the same time introduces symmetry-forbidden dark excitations at low energy. These features can represent the basis for engineering the optical properties of novel curved aromatic molecules.

METHODS AND SYSTEMS

The presented results have been obtained within the framework of Hartree−Fock-based semiempirical methods. All the structures have been optimized through the AM1 model[44] (0.4 kcal mol^{-1}/Å threshold for the forces), which demonstrated its reliability for the investigation of curved aromatics.[45,46] The optical spectra are evaluated by means of ZINDO/S,[47] which implements single-excitation configuration interaction (CIS)[48] and has been validated for C_{60} in the pioneering work by Bendale et al.[42] To highlight the dipolar character of the optical excitations, we introduce the transition density (TD), defined as

$$\rho^I(\mathbf{r}) = \sum_{a,r} c_{ar}^I \phi_r^*(\mathbf{r})\phi_a(\mathbf{r}) \tag{1}$$

where c_{ar}^I are the CI coefficients of the Ith excited state, corresponding to single excitations from the occupied ϕ_a to the virtual ϕ_r molecular orbitals . The sign distribution of this quantity provides a clear pictorial view of the excitation dipole.

In this work we focus on three series of isolated PAHs in gas phase, presenting increasing concavity. In Figure 1 we show the

Received: April 12, 2013
Revised: May 28, 2013
Published: May 30, 2013

   dx.doi.org/10.1021/jp4036259 | J. Phys. Chem. C 2013, 117, 12909−12915

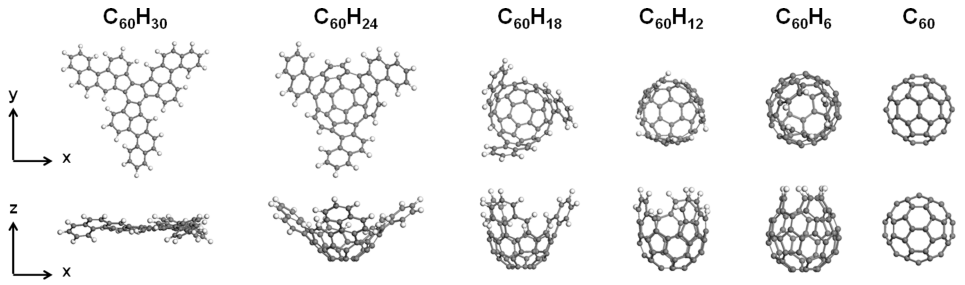

Figure 1. Top (x, y) and side (x, z) view of the $C_{60}H_{6n}$ (n = 0, ..., 5) series of PAHs, related to the formation of icosahedral C_{60} (I_h point group symmetry). At each step, three pairs of H atoms are removed, promoting the π-connectivity of C atoms at the edges and inducing the concavity. The C_3 symmetry of the initial structure $C_{60}H_{30}$ is preserved up to the last intermediate $C_{60}H_6$.

series of $C_{60}H_{6n}$ (n = 0, ..., 5) PAHs, experimentally identified as precursors for an efficient bottom-up synthesis of C_{60}-fullerene catalyzed on a metal surface.[9] These structures contain only hexagons and pentagons and are characterized by a C_3 symmetry, which leads naturally to the 20 hexagons and 12 pentagons of the C_{60} with icosahedral symmetry (I_h point group), upon step-by-step removal of three pairs of H atoms at the periphery. In the process of cage formation the molecules undergo a variation of both concavity and π-connectivity. Concavity is induced by the closure of the network already tailored in the planar $C_{60}H_{30}$, with the progressive formation of pentagons and hexagons. On the other hand, π-connectivity can be quantified as the number of π-bonds formed by each C atom in the molecule. The π-connectivity index rises from 2.5 in $C_{60}H_{30}$, where 30 C atoms out of 60 are H-terminated, up to 3 in the C_{60} molecule, where only C-bonds with π character are present.

RESULTS AND DISCUSSION

In the C_{60} series, depicted in Figure 1, we first notice that a net dipole is acquired by the molecules as soon as the concavity starts to develop: the magnitude of this z-oriented dipole moment is related to the interplay between the extension of the molecule in the out-of-plane direction and the presence of a H-passivated edge. Starting from a negligible intrinsic dipole of the initial planar structure $C_{60}H_{30}$ (μ_z = 0.16 D), which is to be ascribed to the slight distortions of the molecule (see Figure 1), the dipole moment rapidly increases already for the first curved molecule $C_{60}H_{24}$ (μ_z = 7.25 D) and reaches a maximum for $C_{60}H_{18}$ (μ_z = 10.18 D), which presents a π-connectivity index equal to 2.7. As the π-connectivity further increases and the cage progressively closes, the magnitude of the dipole moment starts to decrease (μ_z = 9.71 and 6.22 D for $C_{60}H_{12}$ and $C_{60}H_6$, respectively), eventually vanishing for C_{60}. The process of cage closure described above is also accompanied by an increase of both ionization potential and electron affinity from $C_{60}H_{30}$ to C_{60}. This trend witnesses increasing stabilization and reduced reactivity from the planar H-terminated structure to the fullerene cage. For further details, see Supporting Information Table S1.

In Figure 2 we present the optical spectra of the $C_{60}H_{6n}$ PAH series: the excitations are indicated by solid bars, broadened by a Lorentzian curve with a full width at half-maximum of 100 meV. In the background of each panel we also report the density of CIS states (shaded gray curve), obtained by counting each excitation, irrespective of its oscillator strength (OS), and by applying for visualization a Gaussian broadening with standard deviation of 20 meV. Starting from the spectrum of $C_{60}H_{30}$, the lowest energy excitations appear already at about

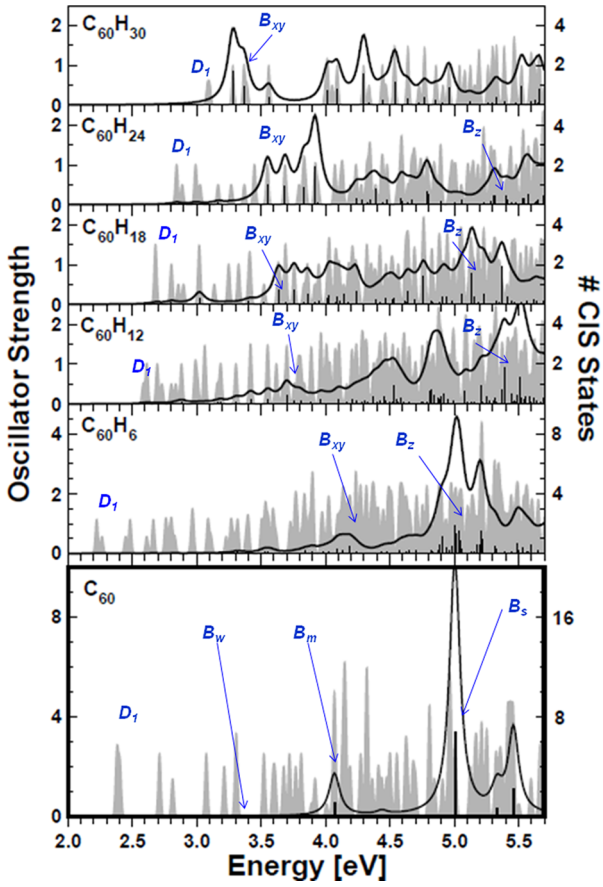

Figure 2. Optical spectra of the $C_{60}H_{6n}$ series: the excitations are indicated by solid bars, and the curves are obtained through a Lorentzian broadening with full width at half-maximum of 100 meV. The density of CIS states shown in the background (gray shaded area) is obtained by counting each excited state with a Gaussian broadening with standard deviation of 20 meV. In each panel the lowest symmetry-forbidden excitation is labeled as D_1: in some spectra more excitations with different symmetry appear summed up to D_1 in the density of CIS states. Bright peaks are indicated as B_{xy} and B_z, depending on their polarization, along the reference directions reported in Figure 1. In the spectrum of C_{60} (bottom panel), bright excitations, which are all triply degenerate, are identified according to their intensity, as in ref 42. B_w is referred to the weakest peak, B_m to a medium-intensity peak, and B_s to the strongest excitation.

3.1 eV: we indicate as D_1 the first symmetry-forbidden excitation (see Table 1 and Figure 3). The first bright peak, labeled as B_{xy}, according to its polarization along the x and y directions, appears at 3.3 eV. This excitation is doubly

dx.doi.org/10.1021/jp4036259 | J. Phys. Chem. C 2013, 117, 12909−12915

Table 1. Energy and Oscillator Strength (OS) of the Main Excitations of the PAH Series $C_{60}H_{6n}$ and of C_{60}, Including the First Symmetry-Forbidden Excitation (D_1) and the Bright Peaks Polarized in the (x, y)-Plane (B_{xy}) and along the z-Direction (B_z)[a]

	D_1		B_{xy}		B_z	
structure	energy [eV]	OS	energy [eV]	OS	energy [eV]	OS
$C_{60}H_{30}$	3.08 (s)	0.00	3.28 (d)	0.84		
$C_{60}H_{24}$	2.89 (s)	0.00	3.55 (d)	0.50	5.54 (s)	0.16
$C_{60}H_{18}$	2.68 (s)	0.00	3.63 (d)	0.37	5.13 (s)	0.76
$C_{60}H_{12}$	2.59 (s)	0.00	3.70 (d)	0.21	5.39 (s)	0.90
$C_{60}H_6$	2.26 (s)	0.00	3.90 (d)	0.01	5.00 (s)	0.94
C_{60}	2.38 (t)	0.00	3.30 (t)	0.0007 (B_w)	5.01 (t)	3.40 (B_s)
			4.07 (t)	0.56 (B_m)		

[a]In the case of C_{60}, we adopt the notation of ref 42 to label the bright peaks. While in C_{60} all the reported excitations present triple (t) degeneracy, in the H-terminated PAHs of this series the indicated excitations present either single (s) or double (d) degeneracy.

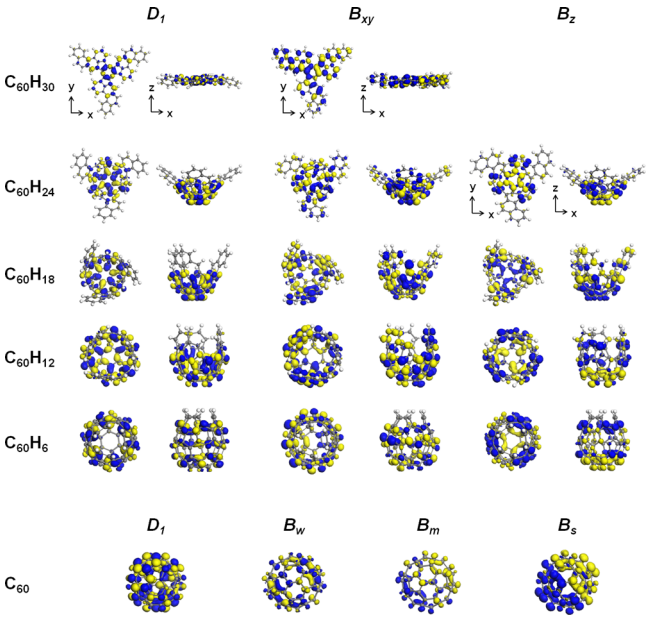

Figure 3. Top (x, y) and side (x, z) views of the transition density plots of the excitations of the $C_{60}H_{6n}$ series (n = 0, ..., 5), as indicated in the spectra of Figure 2.

degenerate, and its strong intensity is given by the large dipole moment in the (x, y) plane (see the transition density plot in Figure 3). Because of the planar structure of $C_{60}H_{30}$, the peaks at higher energy are also (x, y)-polarized.

We can compare the features of $C_{60}H_{30}$ to those of C_{60}, which represents the opposite extreme of the series. Starting with the symmetry-forbidden transitions, in addition to the lowest energy dark excitation (D_1), which is triply degenerate due to the I_h symmetry of fullerene and is now at about 2.3 eV (see Table 1 and Figure 2), many other dark excitations appear in the low-energy region. (For further details in this regard see Table S3 and the related discussion in the Supporting Information.) The allowed absorption peaks are shifted in this case to considerably higher energies: notably, three bright peaks are identified and labeled according to the notation of Bendale et al.,[42] where *weak*, *medium*, and *intense* excitations are mentioned below 5.5 eV. These peaks are indicated in the spectrum of C_{60} in Figure 2 as B_w, B_m, and B_s, respectively, and they are also triply degenerate (see Table 1). B_w is a very weak excitation (OS < 10^{-3}), which is observed at 3.3 eV. A more intense peak (B_m) is visible in the spectrum at about 4.1 eV, while the strongest absorption peak (B_s) is found at 5 eV. The sign modulation of the transition density of B_w clearly explains the low intensity of this excitation (see Figure 3). On the contrary, the transition densities associated with B_m and B_s present separate domains of opposite sign. For a given value of isosurface (8×10^{-4} in this case), the higher intensity of B_s compared to B_m can be visualized in the plots in Figure 3. Comparing our results with those presented by Bendale and co-workers,[42] we notice a good agreement with the excitation energies obtained for a comparable CI window.[49] A thorough comparison with the experimental data taken from ref 43 is presented in the discussion of Figure 4.

Focusing now on the series behavior reported in Figure 2, we observe a blue-shift of the intense absorption lines and a red-shift of the lowest energy dark state D_1, with the appearance of an increasingly large number of forbidden excitations in between. These features are due to the increase of both concavity and π-connectivity, triggered by the dehydrogenation process in the formation of the fullerene cage. The increase of π-connectivity leads to a larger delocalization of the molecular orbitals (MOs), which is responsible for the general red-shift of the density of forbidden or very weak CIS states (see Figure 2, from the top to the bottom panel).[50]

The first bright peak B_{xy}, observed for $C_{60}H_{30}$, is easily recognized for $C_{60}H_{24}$ and for $C_{60}H_{18}$ as the first intense peak in the spectrum. For $C_{60}H_{12}$ and $C_{60}H_6$ the identification of B_{xy} is less immediate, since the low-energy part of their spectra is characterized by a large number of low-intensity peaks polarized in the (x, y) plane. In the spectra of these molecules B_{xy} is chosen for the similarity of the transition density with respect to the less concave structures $C_{60}H_{24}$ and $C_{60}H_{18}$ (see the plots in Figure 3 and Table 1 for the trends of energy and OS). On the other hand, the intensity of the absorption increases for more concave molecules at higher energy. In this region the most intense peaks present a z-polarization. B_z is identified in the spectra as the first z-polarized peak: the orientation of its excitation dipole is evident in the transition density plots in Figure 3. A remarkable similarity between the spectra of $C_{60}H_6$ and C_{60} is noticed, suggesting that the intense B_z peak in the former molecule eventually becomes the strong B_s peak in C_{60}.

The optical features discussed for the $C_{60}H_{6n}$ series are apparent also for another set of PAHs, namely pentaindenocorannulene ($C_{50}H_{20}$) and the [5,5]-CNT-cap ($C_{50}H_{10}$). Both these structures have been experimentally synthesized in the past few years, as crystal-packed structures in solution.[10,14,16] Differently from the structures of the $C_{60}H_{6n}$ series, these systems have not been produced as subsequent synthesis steps, although clear perspectives in this sense are suggested in the

dx.doi.org/10.1021/jp4036259 | J. Phys. Chem. C 2013, 117, 12909−12915

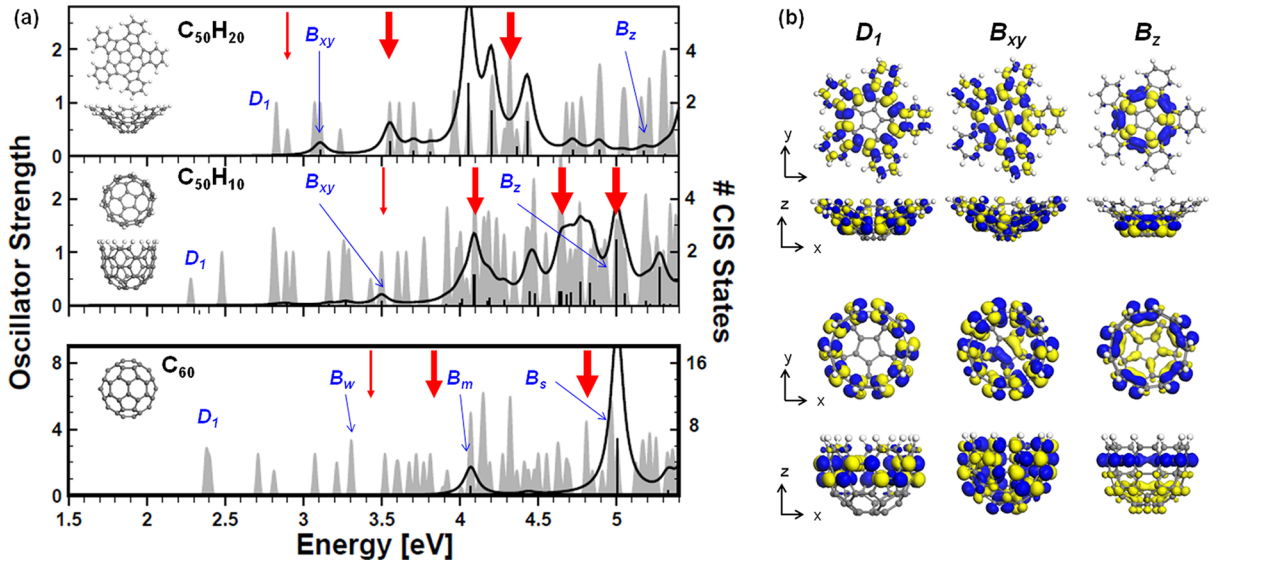

Figure 4. (a) Optical spectra of pentaindenocorannulene ($C_{50}H_{20}$) and of the related CNT-cap ($C_{50}H_{10}$), shown in the inset; for comparison, the spectrum of C_{60} is displayed on the bottom panel. In analogy with the $C_{60}H_{6n}$ series, shown in Figure 2, also in the spectra of $C_{50}H_{20}$ and $C_{50}H_{10}$ the lowest dark excitation (D_1) as well as the first bright peaks (B_{xy} and B_z) are marked. The excitations are indicated by solid bars and the curves are obtained through a Lorentzian curve with full width at half-maximum of 100 meV. The gray shaded lines represent the density of CIS states (Gaussian broadening with standard deviation of 20 meV). Red arrows point to the energy of optical peaks observed experimentally[10,14,42] for $C_{50}H_{20}$, $C_{50}H_{10}$, and C_{60}, respectively. The thickness of the arrows indicates of the intensity of the detected excitations. (b) Top (x, y) and side (x, z) view of the transition densities associated with D_1, B_{xy}, and B_z for $C_{50}H_{20}$ (top) and $C_{50}H_{10}$ (bottom).

outlook of ref 16. Both pentaindenocorannulene and the CNT-cap belong to C_{5v} point group symmetry and are characterized by the same central corannulene unit (see insets in Figure 4a), which represents the starting point in the process of synthesis of both $C_{50}H_{20}$[14] and $C_{50}H_{10}$.[10] Because of the similarities between these structures and the increasing π-connectivity and concavity from $C_{50}H_{20}$ to $C_{50}H_{10}$, it is reasonable to carry out an analytical comparison of their optical properties, in analogy with the $C_{60}H_{6n}$ series. The trends observed for this set of PAHs are in agreement with the $C_{60}H_{6n}$ series, concerning the electronic and optical properties. Both $C_{50}H_{20}$ and $C_{50}H_{10}$ are characterized by a dipole moment in the out-of-plane z-direction (μ_z = 2.59 and 8.98 D, respectively). In analogy with the $C_{60}H_{6n}$ series, we observe increasing ionization potential and electron affinity from $C_{50}H_{20}$ to the CNT-cap, as a consequence of larger electronic stability at higher π-connectivity index (2.6 for $C_{50}H_{20}$ and 2.8 for $C_{50}H_{10}$). Further details are provided in the Supporting Information Table S2.

The optical spectra of these molecules are shown in Figure 4a, in comparison with the spectrum of the closed-cage C_{60}, reported for reference. As for the case of the $C_{60}H_{6n}$ series, we identify in the spectra the excitations labeled as D_1, B_{xy}, and B_z, in addition to a number of dark states lying between D_1 and the first active peak. The energy of the first excitation decreases from $C_{50}H_{20}$ to the CNT-cap, on account of the increased π-connectivity. On the other hand, the energy of bright peaks blue-shifts in the spectrum of the cap. B_{xy} is identified in the spectra of both $C_{50}H_{20}$ and $C_{50}H_{10}$ as the lowest energy doubly degenerate peak polarized in the (x, y) plane (see the transition densities in Figure 4b). The intensity of B_z grows by 1 order of magnitude from $C_{50}H_{20}$ to $C_{50}H_{10}$ due to the more extended C-conjugated network along the z direction in the CNT-cap. For further details, see Table S4.

The computed spectra of $C_{50}H_{20}$ and $C_{50}H_{10}$ are compared in Figure 4a with the available experimental data presented in the Supporting Information of refs 10 and 14, respectively. In both cases the spectra are recorded in CH_2Cl_2 solution. The experimentally detected energy of the main peaks is indicated in Figure 4a by the position of red arrows, and their intensity is represented by the thickness of the arrows. By inspecting Figure 4a, a generally good agreement between our results and the available experimental data is shown, concerning both the energy and the strength of the intense peaks. Our study represents the first theoretical investigation on the optical properties of pentaindenocorannulene $C_{50}H_{20}$ and of the CNT-cap $C_{50}H_{10}$, and we are hopeful that it can further stimulate the interest in the interaction of these molecules with light, also from the experimental viewpoint.

In the bottom panel of Figure 4a we report the optical spectrum of C_{60}, in comparison with the experimental UV−vis spectrum of ref 43, as discussed also in ref 42. In our calculations, the *medium* (B_m) and *strong* (B_s) peaks at 4 and 5 eV result almost systematically blue-shifted of about 200 meV compared to the experimental spectra, taken in hexane solution.[43] As for the *weak* peak B_w, detected at 3.4 eV, it is predicted by our calculations to be at 3.3 eV. It is worth noting that the lowest energy excitations, which are indicated as dark by symmetry in our ZINDO/S spectrum, are actually observed in the experimental spectra. This testifies that the manifold of dark excitations in the low-energy region of the spectra of concave PAHs can be activated in experiments, due to a loss of symmetry of the molecules, as it likely occurs in solution or under other laboratory conditions.

As a last example, we discuss a third class of PAHs, where the five-member rings are not included in the initial structure but tend to form in defective graphene flakes, as shown in Figure 5a. These structures are inspired by those presented in ref 41. In that work, the formation of C_{60} from a graphene sheet is visualized in real time through a transmission electron microscope. The process is modeled in four steps: the initial edge etching of a graphene flake with over 80 C atoms is followed by the formation of pentagons and then by the curving

dx.doi.org/10.1021/jp4036259 | J. Phys. Chem. C 2013, 117, 12909−12915

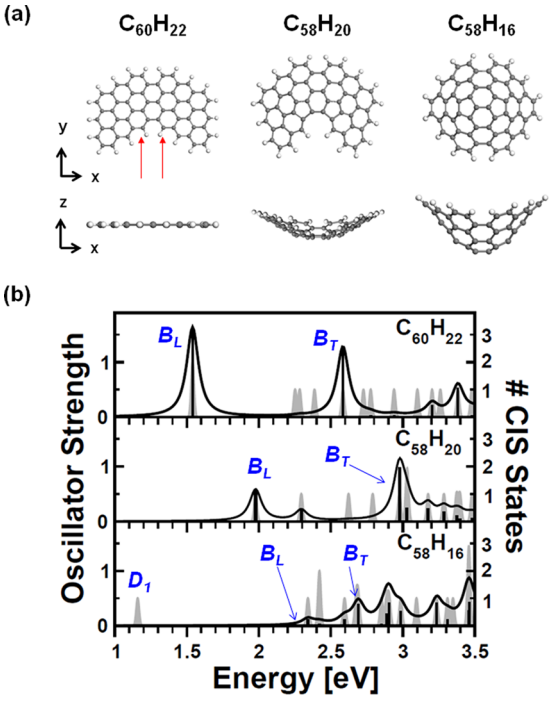

Figure 5. (a) Top (x, y) and side view (x, z) of planar ($C_{60}H_{22}$), etched ($C_{58}H_{20}$), and zipped ($C_{58}H_{16}$) PAHs. The structure of $C_{58}H_{20}$ is obtained by removing the two C atoms, and the corresponding saturating H atoms, in the cove region of $C_{60}H_{20}$ (see red arrows). Two pentagons are formed in $C_{60}H_{22}$, and next, after the removal of 4 H atoms at the edges, the flake is zipped through the bonding of the unsaturated C atoms. (b) Optical spectra of the systems shown in (a): the excitations are indicated by solid bars, and the curves are obtained by adding a Lorentzian broadening with fwhm of 100 meV. The density of CIS states (Gaussian broadening with standard deviation of 20 meV) is indicated in the background of each panel by the gray shaded area. In the spectrum of the planar $C_{60}H_{22}$ the first bright peaks are labeled as B_L and B_T, according to their longitudinal (along x axis) and transverse (along z axis) polarization, respectively. The corresponding excitations are indicated also in the spectra of the etched $C_{58}H_{20}$ and zipped $C_{58}H_{16}$.

of the graphene into a bowl-shape structure. Finally, the open edges are zipped up to form a closed fullerene structure. We here model the etching and zipping of graphene samples using H-passivated graphene flakes with about 60 C atoms, for comparison with the $C_{60}H_{6n}$ series of fullerene precursors. Starting from an initially planar structure ($C_{60}H_{22}$, Figure 5a), two C atoms are removed by etching and two pentagons are formed in the $C_{58}H_{20}$ intermediate molecule, introducing concavity. The molecule is finally zipped after the removal of 4 H atoms at the cove edge and the subsequent bonding of the unsaturated C atoms. No additional pentagons are formed in this process, and the resulting $C_{58}H_{16}$ assumes a bowl-like shape. The initial structure $C_{60}H_{22}$ and the zipped flake $C_{58}H_{16}$ present C_{2v} symmetry, which are however related to different rotation axes. While $C_{60}H_{22}$ is symmetric for rotation with respect to the y axis, the symmetry axis of $C_{58}H_{16}$ is in the z direction (see Figure 5a).

The optical spectra of this set of structures are shown in Figure 5b. For the planar $C_{60}H_{22}$ the low-energy region of the spectrum is characterized by two intense peaks polarized in the longitudinal (x) and transverse (y) direction of the molecules (B_L and B_T, respectively), similarly to the situation of H-terminated armchair graphene nanoribbons with finite length.[51] B_L and B_T are identified also in the spectrum of $C_{58}H_{20}$, and their polarization directions are preserved even after the formation of pentagons. An overall blue-shift of the spectrum of $C_{58}H_{20}$ is observed compared to that of $C_{60}H_{22}$: it is induced by the increased concavity acquired by the molecule after the etching. This behavior confirms the picture drawn for the $C_{60}H_{6n}$ series. The intensity of B_L, dominated by a HOMO → LUMO transition, decreases as the extension of $C_{58}H_{20}$ in the x direction is reduced; on the other hand, the intensity of B_T is basically preserved from $C_{60}H_{22}$ to $C_{58}H_{20}$. The edge zipping from $C_{58}H_{20}$ to $C_{58}H_{16}$ contributes to the increase of both concavity and π-connectivity, whose index raises from about 2.66 to about 2.72. As a consequence of the induced concavity, the first bright peak B_L is blue-shifted (see Figure 5b) and its OS is reduced, owing to the smaller extension of the flake along the polarization direction x. As an effect of π-connectivity, we note an interesting behavior of the occupied MOs, which leads to the appearance in the spectrum of $C_{58}H_{16}$ of a symmetry forbidden state (D_1) at very low energy. This excitation is due to the HOMO → LUMO transition, but in this case the HOMO has the same character of the HOMO-3 of $C_{58}H_{20}$, which moves here to higher energy with respect to the other two MOs, due to the increased π-connectivity.

CONCLUSIONS

In conclusion, we have examined three families of experimentally feasible PAHs, related to the formation of concave C-allotropes (including C_{60} and C_{50}-CNT-caps), having different underlying symmetry and increasing concavity and π-connectivity. The interplay between these properties is responsible for a general blue-shift of the optical absorption and for the appearance of a number of dark excitations at low energy, specifically in the visible region of the spectrum, which are forbidden by symmetry. The high-energy optical modes polarized in the out-of-plane direction gain oscillator strength due to the increasing concavity and to the presence of a H-passivated edge. On the other hand, the excitations polarized in the (x, y) plane, which dominate the spectra of the planar structures, are considerably less intense. At the same time, as expected, the increase of π-connectivity tends to reduce the energy of the first excited configurations. The resulting lowest-energy states are dark, but they may however be experimentally detected due to overall symmetry loosening of the structure.

The trends observed in our results are mainly based on general symmetry and topology arguments and can therefore represent the basis for engineering the optical properties of novel curved aromatic molecules. These features are observed in all the considered PAH series and are supported by a good agreement with the available experimental data. For most of the considered systems, the results presented here are the first theoretical study on the optical properties. We believe that our detailed analysis on the excitations, with specific attention devoted to the dark states in the visible range, will further stimulate the interest in curved PAHs and specifically in their interaction with light.

ASSOCIATED CONTENT

Supporting Information

Computed electron affinity and ionization potential for the $C_{60}H_{6n}$ series and the details of the optical excitations (i.e., excitation energies and oscillator strength as well as transition density plots) of C_{60}, $C_{50}H_{20}$, and $C_{50}H_{10}$ and zipped PAHs.

dx.doi.org/10.1021/jp4036259 | J. Phys. Chem. C 2013, 117, 12909−12915

This material is available free of charge via the Internet at http://pubs.acs.org.

AUTHOR INFORMATION

Corresponding Author

*E-mail: caterina.cocchi@unimore.it.

Present Address

[⊥]C.C.: Humboldt-Universität zu Berlin, Institut für Physik and IRIS Adlershof, Zum GrossenWindkanal 6, 12489 Berlin, Germany.

Notes

The authors declare no competing financial interest.

ACKNOWLEDGMENTS

The authors are grateful to Lennert van Tilburg for useful discussions. This work was partly supported by the Italian Ministry of University and Research under FIRB grant ItalNanoNet and by Fondazione Cassa di Risparmio di Modena with project COLDandFEW. M.J.C. acknowledges support from FAPESP and CNPq (Brazil).

REFERENCES

(1) Kroto, H. W.; Allaf, A. W.; Balm, S. P. C_{60}: Buckminsterfullerene. *Chem. Rev.* **1991**, *91*, 1213−1235.

(2) Iijima, S. Helical Microtubules of Graphitic Carbon. *Nature (London)* **1991**, *354*, 56−58.

(3) Novoselov, K. S.; Geim, A. K.; Morozov, S. V.; Jiang, D.; Zhang, Y.; Dubonos, S. V.; Grigorieva, I. V.; Firsov, A. A. Electric Field Effect in Atomically Thin Carbon Films. *Science* **2004**, *306*, 666−669.

(4) *Science of Fullerenes and Carbon Nanotubes: Their Properties and Applications*; Dresselhaus, G., Dresselhaus, M. S., Eklund, P. C., Eds.; Academic: New York, 1996.

(5) Katsnelson, M. *Graphene: Carbon in Two Dimensions*; Cambridge University Press: New York, 2012.

(6) Hoheisel, T.; Schrettl, S.; Szilluweit, R.; Frauenrath, H. Nanostructured Carbonaceous Materials from Molecular Precursors. *Angew. Chem., Int. Ed.* **2010**, *49*, 6496−6515.

(7) Boorum, M. M.; Vasil'ev, Y. V.; Drewello, T.; Scott, L. T. Groundwork for a Rational Synthesis of C_{60}: Cyclodehydrogenation of a $C_{60}H_{30}$ Polyarene. *Science* **2001**, *294*, 828−831.

(8) Yu, X.; Zhang, J.; Choi, W.; Choi, J.; Kim, J.; Gan, L.; Liu, Z. Cap Formation Engineering: From Opened C_{60} to Single-Walled Carbon Nanotubes. *Nano Lett.* **2010**, *10*, 3343−3349.

(9) Amsharov, K.; Abdurakhmanova, N.; Stepanow, S.; Rauschenbach, S.; Jansen, M.; Kern, K. Towards the Isomer-Specific Synthesis of Higher Fullerenes and Buckybowls by the Surface-Catalyzed Cyclodehydrogenation of Aromatic Precursors. *Angew. Chem., Int. Ed.* **2010**, *122*, 9582−9586.

(10) Scott, L. T.; Jackson, E. A.; Zhang, Q.; Steinberg, B. D.; Bancu, M.; Li, B. A Short, Rigid, Structurally Pure Carbon Nanotube by Stepwise Chemical Synthesis. *J. Am. Chem. Soc.* **2012**, *134*, 107−110.

(11) Tsefrikas, V.; Scott, L. Geodesic Polyarenes by Flash Vacuum Pyrolysis. *Chem. Rev.* **2006**, *106*, 4868−4884.

(12) Wu, Y.-T.; Siegel, J. S. Aromatic Molecular-Bowl Hydrocarbons: Synthetic Derivatives, Their Structures, and Physical Properties. *Chem. Rev.* **2006**, *106*, 4843−4867.

(13) Kawase, T.; Kurata, H. Ball-, Bowl-, and Belt-Shaped Conjugated Systems and Their Complexing Abilities: Exploration of the Concave-Convex *pi-pi* Interaction. *Chem. Rev.* **2006**, *106*, 5250−5273.

(14) Jackson, E.; Steinberg, B.; Bancu, M.; Wakamiya, A.; Scott, L. Pentaindenocorannulene and Tetraindenocorannulene: New Aromatic Hydrocarbon π Systems with Curvatures Surpassing That of C60. *J. Am. Chem. Soc.* **2007**, *129*, 484−485.

(15) Mack, J.; Vogel, P.; Jones, D.; Kaval, N.; Sutton, A. The Development of Corannulene-Based Blue Emitters. *Org. Biomol. Chem.* **2007**, *5*, 2448−2452.

(16) Steinberg, B. D.; Jackson, E. A.; Filatov, A. S.; Wakamiya, A.; Petrukhina, M. A.; Scott, L. T. Aromatic p-Systems More Curved Than C60. The Complete Family of All Indenocorannulenes Synthesized by Iterative Microwave-Assisted Intramolecular Arylations. *J. Am. Chem. Soc.* **2009**, *131*, 10537−10545.

(17) Whalley, A.; Plunkett, K.; Gorodetsky, A.; Schenck, C.; Chiu, C.; Steigerwald, M.; Nuckolls, C. Bending Contorted Hexabenzocoronene into a Bowl. *Chem. Sci.* **2011**, *2*, 132−135.

(18) Berné, O.; Tielens, A. Formation of Buckminsterfullerene (C_{60}) in Interstellar Space. *Proc. Natl. Acad. Sci. U. S. A.* **2012**, *109*, 401−406.

(19) Forkey, D. M.; Attar, S.; Noll, B. C.; Koerner, R.; Olmstead, M. M.; Balch, A. L. Crystallographic Characterization of the Molecular Structure and Solid State Packing of the Fullerene-Shaped Hydrocarbon $C_{36}H_{12}$. *J. Am. Chem. Soc.* **1997**, *119*, 5766−5767.

(20) Xiao, W.; Passerone, D.; Ruffieux, P.; Ait-Mansour, K.; Gröning, O.; Tosatti, E.; Siegel, J. S.; Fasel, R. C_{60}/Corannulene on Cu(110): A Surface-Supported Bistable Buckybowl-Buckyball Host-Guest System. *J. Am. Chem. Soc.* **2008**, *130*, 4767−4771.

(21) Pérez, E.; Martín, N. Curves Ahead: Molecular Receptors for Fullerenes Based on Concave−Convex Complementarity. *Chem. Soc. Rev.* **2008**, *37*, 1512−1519.

(22) Sygula, A.; Fronczek, F. R.; Sygula, R.; Rabideau, P. W.; Olmstead, M. M. A Double Concave Hydrocarbon Buckycatcher. *J. Am. Chem. Soc.* **2007**, *129*, 3842−3843.

(23) Wu, Y.-T.; Bandera, D.; Maag, R.; Linden, A.; Baldridge, K. K.; Siegel, J. S. Multiethynyl Corannulenes: Synthesis, Structure, and Properties. *J. Am. Chem. Soc.* **2008**, *130*, 10729−10739.

(24) Baldridge, K. K.; Hardcastle, K. I.; Seiders, T. J.; Siegel, J. S. Synthesis, Structure and Properties of Decakis-(Phenylthio)-Corannulene. *Org. Biomol. Chem.* **2010**, *8*, 53−55.

(25) Tremblay, N.; Gorodetsky, A.; Cox, M.; Schiros, T.; Kim, B.; Steiner, R.; Bullard, Z.; Sattler, A.; So, W.; Itoh, Y.; Tremblay, N. J.; Gorodetsky, A. A.; Cox, M. P.; Schiros, T.; Kim, B.; Steiner, R.; Bullard, Z.; Sattler, A.; So, W. Y.; Itoh, Y.; et al. Photovoltaic Universal Joints: Ball-and-Socket Interfaces in Molecular Photovoltaic Cells. *ChemPhysChem* **2010**, *11*, 799−803.

(26) Zoppi, L.; Martin-Samos, L.; Baldridge, K. Effect of Molecular Packing on Corannulene-Based Materials Electroluminescence. *J. Am. Chem. Soc.* **2011**, *133*, 14002−14009.

(27) Osella, S.; Narita, A.; Schwab, M. G.; Hernandez, Y.; Feng, X.; Müllen, K.; Beljonne, D. Graphene Nanoribbons as Low Band Gap Donor Materials for Organic Photovoltaics: Quantum Chemical Aided Design. *ACS Nano* **2012**, *6*, 5539−5548.

(28) Prezzi, D.; Varsano, D.; Ruini, A.; Marini, A.; Molinari, E. Optical Properties of Graphene Nanoribbons: The Role of Many-Body Effects. *Phys. Rev. B* **2008**, *77*, 041404(R).

(29) Jiang, J.; Lu, W.; Bernholc, J. Edge States and Optical Transition Energies in Carbon Nanoribbons. *Phys. Rev. Lett.* **2008**, *101*, 246803.

(30) Li, Y.; Gao, J.; Di Motta, S.; Negri, F.; Wang, Z. Tri-N-annulated Hexarylene: An Approach to Well-Defined Graphene Nanoribbons with Large Dipoles. *J. Am. Chem. Soc.* **2010**, *132*, 4208−4213.

(31) Zhu, X.; Su, H. Excitons of Edge and Surface Functionalized Graphene Nanoribbons. *J. Phys. Chem. C* **2010**, *114*, 17257−17262.

(32) Wang, H.; Su, H.; Qian, H.; Wang, Z.; Wang, X.; Xia, A. Structure-Dependent All-Optical Switching in Graphene-Nanoribbon-Like Molecules: Fully Conjugated Tri-(Perylene Bisimides). *J. Phys. Chem. A* **2010**, *114*, 9130.

(33) Cocchi, C.; Ruini, A.; Prezzi, D.; Caldas, M. J.; Molinari, E. Designing All-Graphene Nanojunctions by Covalent Functionalization. *J. Phys. Chem. C* **2011**, *115*, 2969−2973.

(34) Cocchi, C.; Prezzi, D.; Ruini, A.; Caldas, M.; Molinari, E. Optical Properties and Charge-Transfer Excitations in Edge-Functionalized All-Graphene Nanojunctions. *J. Phys. Chem. Lett.* **2011**, *2*, 1315−1319.

(35) Prezzi, D.; Varsano, D.; Ruini, A.; Molinari, E. Quantum Dot States and Optical Excitations of Edge-Modulated Graphene Nanoribbons. *Phys. Rev. B* **2011**, *84*, 041401.

(36) Wang, S.; Wang, J. Quasiparticle Energies and Optical Excitations in Chevron-Type Graphene Nanoribbon. *J. Phys. Chem. C* **2012**, *116*, 10193−10197.
(37) Caetano, E. W. S.; Freire, V. N.; dos Santos, S. G.; Albuquerque, E. L.; Galvaõ, D. S.; Sato, F. Defects in Graphene-Based Twisted Nanoribbons: Structural, Electronic, and Optical Properties. *Langmuir* **2009**, *25*, 4751−4759.
(38) Wong, B. M. Optoelectronic Properties of Carbon Nanorings: Excitonic Effects from Time-Dependent Density Functional Theory. *J. Phys. Chem. C* **2009**, *113*, 21921−21927.
(39) Rieger, R.; Müllen, K. Forever Young: Polycyclic Aromatic Hydrocarbons as Model Cases for Structural and Optical Studies. *J. Phys. Org. Chem.* **2010**, *23*, 315−325.
(40) Cocchi, C.; Prezzi, D.; Ruini, A.; Caldas, M. J.; Molinari, E. Electronics and Optics of Graphene Nanoflakes: Edge Functionalization and Structural Distortions. *J. Phys. Chem. C* **2012**, *116*, 17328−17335.
(41) Chuvilin, A.; Kaiser, U.; Bichoutskaia, E.; Besley, N.; Khlobystov, A. Direct Transformation of Graphene to Fullerene. *Nat. Chem.* **2010**, *2*, 450−453.
(42) Bendale, R.; Baker, J.; Zerner, M. Calculations on the Electronic Structure and Spectroscopy of C_{60} and C_{70} Cage Structures. *Int. J. Quantum Chem.* **1991**, *40*, 557−568.
(43) Ajie, H.; Alvarez, M. M.; Anz, S. J.; Beck, R. D.; Diederich, F.; Fostiropoulos, K.; Huffman, D. R.; Kraetschmer, W.; Rubin, Y.; et al. Characterization of the Soluble All-Carbon Molecules C_{60} and C_{70}. *J. Phys. C* **1990**, *94*, 8630−8633.
(44) Dewar, M. J. S.; Zoebish, E. G.; Healy, E. F.; Stewart, J. J. P. A New General Purpose Quantum Mechanical Molecular Model. *J. Am. Chem. Soc.* **1985**, *107*, 3902−3909.
(45) Dinadayalane, T.; Narahari Sastry, G. An Assessment of Semiempirical (MNDO, AM1 and PM3) Methods to Model Buckybowls. *J. Mol. Struct.* **2002**, *579*, 63−72.
(46) Petrukhina, M. A.; Andreini, K. W.; Mack, J.; Scott, L. T. X-Ray Quality Geometries of Geodesic Polyarenes from Theoretical Calculations: What Levels of Theory Are Reliable? *J. Org. Chem.* **2005**, *70*, 5713−5716.
(47) Ridley, J.; Zerner, M. An Intermediate Neglect of Differential Overlap Techinique for Spectroscopy: Pyrrole and the Azines. *Theor. Chim. Acta* **1973**, *32*, 111−134.
(48) AM1 and ZINDO/S calculations were performed using VAMP package included in Accelrys Materials Studio software, version 6.0 (http://accelrys.com/products/materials-studio). Our convergence tests over a number of occupied and virtual molecular orbitals (MOs) indicated that a CI energy window of at least 4.5 eV below the HOMO and 3.5 eV above the LUMO is required for a reliable characterization of the low-energy optical excitations.
(49) Our calculations were performed including 38 occupied and 37 empty states, which correspond to an energy window of 6.9 eV below HOMO and 5.5 eV above LUMO. This CI window is compatible with that including 30 occupied and 35 empty states in ref 42, and indeed the two sets of results are consistent (see Table 1 for detailed comparison). According to the results of Bendale et al., only B_w and B_m are convergent within a threshold of 100 meV with respect to the largest employed CI window, with 111 occupied and 109 empty states.[42] The strongest peak at about 5 eV undergoes a shift of over 300 meV between the 30 × 35 and 111 × 109 CI windows.[42] Further slight discrepancies between our results and those obtained in ref 42 can be ascribed to the differently optimized geometries: AM1 is adopted here, while Bendale et al. make use of the INDO/1 Hamiltonian. The resulting lengths of pentagon−hexagon and hexagon−hexagon bonds are 1.464 and 1.398 Å, which are 0.013 Å larger and shorter, respectively, than those computed in ref 42.
(50) In the $C_{60}H_{6n}$ series D_1 is found energetically close (few tens of meV) to a pair of doubly degenerate excitations polarized in the (x, y) plane, with very weak but nonzero intensity (OS ∼ 10^{-4}−10^{-2}). It is worth noting that this behavior finally leads to manifolds of triply degenerate excitations in C_{60}. In the case of $C_{60}H_{24}$, $C_{60}H_{18}$, and $C_{60}H_6$, the excitation D_1 corresponds to the third excited state in the spectrum, as a pair of doubly degenerate excitation is found at lower energy.
(51) Cocchi, C.; Prezzi, D.; Ruini, A.; Benassi, E.; Caldas, M. J.; Corni, S.; Molinari, E. Optical Excitations and Field Enhancement in Short Graphene Nanoribbons. *J. Phys. Chem. Lett.* **2012**, *3*, 924−929.